



ORIGINAL ARTICLE

Cytotoxicity assay of plant-mediated synthesized iron oxide nanoparticles using *Juglans regia* green husk extract



Zahra Izadiyan^a, Kamyar Shameli^{a,*}, Mikio Miyake^a, Hirofumi Hara^a, Shaza Eva Binti Mohamad^a, Katayoon Kalantari^b, Siti Husnaa Mohd Taib^a, Elisa Rasouli^c

^a Department of Environment and Green Technology, Malaysia-Japan International Institute of Technology, Universiti Teknologi Malaysia, Jalan Sultan Yahya Petra, 54100 Kuala Lumpur, Malaysia

^b Centre of Advanced Materials (CAM), Faculty of Engineering, University of Malaya, 50603 Kuala Lumpur, Malaysia

^c Nanotechnology & Catalysis Research Centre, Institute of Postgraduate Studies, University Malaya, 50603 Kuala Lumpur, Malaysia

Received 28 August 2017; accepted 26 February 2018
Available online 10 March 2018

KEYWORDS

Iron oxide nanoparticles;
Green synthesis;
Juglans regia;
Green husk;
Cytotoxicity assay

Abstract Synthesis of iron oxide nanoparticles has attracted increasing interest due to their importance in biomedical and technological applications. To investigate the ability of *Juglans regia* (*J. regia*) green husk extract in iron oxide nanoparticles size control, they were synthesized through co-precipitation method with *J. regia* extract and without it. For both tests, other experimental conditions were same. According to High-resolution transmission electron microscopy, the mean diameter and standard deviation of iron oxide nanoparticles and *J. regia*/iron oxide nanoparticles synthesized using co-precipitation method were 12.60 ± 2.87 and 5.77 ± 1.66 nm respectively. These results showed that *J. regia*/iron oxide nanoparticles synthesized using extract have a smaller size than nanoparticles fabricated by co-precipitation method; moreover, green husk extract plays the main role as size control. The obtained results of Powder X-ray diffraction (PXRD), High resolution transmission electron microscopy (HR-TEM), Field emission scanning electron microscopy (FESEM), and Energy dispersive X-ray (EDX) are in good agreement with each other and confirm the high purity of fabricated magnetic nanoparticles using *J. regia* extract. Vibrating sample magnetometer (VSM) revealed that the *J. regia*/iron oxide nanoparticles due to their proper magnetic

* Corresponding author.

E-mail addresses: zahra_izadiyan@yahoo.com.my (Z. Izadiyan), kamyarshameli@gmail.com (K. Shameli), miyake@utm.my (M. Miyake), hhara@utm.my (H. Hara), shaza@utm.my (S.E.B. Mohamad), Katayoon@um.edu.my (K. Kalantari), shmt1988@gmail.com (S.H.M. Taib), elisa.rasouli@gmail.com (E. Rasouli).

Peer review under responsibility of King Saud University.



Production and hosting by Elsevier

properties have high saturation magnetization and low coercivity. According to FTIR spectrum, the *J. regia* would be coated on the iron oxide nanoparticles surface in a successful manner. The non-toxic effect of *J. regia*/iron oxide nanoparticles concentration below 1000 µg/ml was observed in the studies of in vitro cytotoxicity on normal and cancerous cell lines, respectively. The dose-dependent toxicity made it a suitable candidate for various medical applications.

© 2018 Production and hosting by Elsevier B.V. on behalf of King Saud University. This is an open access article under the CC BY-NC-ND license (<http://creativecommons.org/licenses/by-nc-nd/4.0/>).

1. Introduction

Current development of nanotechnology has an advantage in the nanoscience field and it has become popular in the past twenty years. Nanoparticles are generally defined as particles with a measurement of 100 nm or less in diameter with the particular feature that mainly size-dependent (Darezereshki et al., 2010). Research on nanoparticles has become attractive due to its superior and unique characteristics as opposed to other materials that had led to their application in a wide array of fields (Shameli et al., 2012). Some of these characteristics or properties include the thermal, catalytic, and optical properties as well as being an electrical conductor and in use for biological applications (Shameli et al., 2010a). The attractive properties are the result of its high surface energy as well as a high ratio in the surface to volume with comparatively minute sizes. The nanoparticles' synthesis in the polymeric media has shown promise due to the processing ease, solubility, less toxicity, with the potential to control the resulting nanoparticles' growth (Shameli et al., 2010b).

Nanoparticles are widely used in biomedical applications such as anticancer, antimicrobial, mosquitocidal (Benelli, 2016a; Benelli et al., 2016; Dinesh et al., 2015), antiplasmodial (Govindarajan and Benelli, 2017), larvicidal (Vincent et al., 2017), ovicidal and larvicidal potential for malaria, dengue and filariasis mosquito Vectors (Govindarajan et al., 2016; Murugan et al., 2015). They also have potential application in other fields such as for enhanced photocatalytic performance (Zhang et al., 2017), removal (Huang et al., 2017; Kalantari et al., 2015), anodes for lithium-Ion Batteries (Lou et al., 2017), and high-performance dye-sensitized solar cells (Liu et al., 2017). In addition, it synthesized nanoparticles as inhibitors of green, dengue growth (Benelli, 2016b). Several nanoparticles can be used for various medical applications such as iron oxide nanoparticles with suitable surface chemistry, immunoassay, tissue repair detoxification of biological fluids, cell sorting and hyperthermia (Gupta and Gupta, 2005), MRI contrast enhancement (Burtea et al., 2005), cancer therapy (Pardoe et al., 2003), and targeted drug delivery (Chourpa et al., 2005). Cancer is one of the major global health problems and involves uncontrolled cell growth with striking changes in biochemical and enzymatic parameters (Kuppusamy et al., 2016). Surgery, chemotherapy, radiation, immunotherapy, and hormones are the main treatments for cancer, but chemotherapy is used predominantly. However, chemotherapy not only kills cancer cells, but also affects normal cells. All of these treatment methods are expensive and may have limited efficacy, toxicity or chance for multiple drug resistance (Istudor, 2004; Tan et al., 2011).

Nanoparticles are a few hundred nanometers smaller than comparable large biological molecules (enzymes, receptors

and antibodies). These nanoparticles, which are 100–10,000 times smaller in size than human cells, can present unprecedented interactions between both the biological molecules and the cells on the surface and within the cells. Nanoparticle therapy can be revolutionary in the diagnosis and treatment of cancer (Seigneuric et al., 2010).

There are various methods for the synthesis of iron oxide nanoparticles such as sol-gel reactions (Bagheri et al., 2013), sonochemical (Abdullah et al., 2017; Vijayakumar et al., 2000), hydrothermal methods (Giri et al., 2005), microemulsion process (Vidal-Vidal et al., 2006), flow injection synthesis (Salazar-Alvarez et al., 2006), radiolysis (Abedini et al., 2014), microwave methods (Carenza et al., 2014), aerosol pyrolysis (Tartaj et al., 2004), and laser pyrolysis (Bomatí-Miguel et al., 2008). When synthesized by chemical and physical methods, these nanoparticles lose their reactivity due to aggregation of air exposure (Kim et al., 2008), magnetism, and dispersibility (Wu et al., 2008). Chemical synthesis methods involve contamination from toxic chemicals, formation of dangerous by-products, and chemical precursors (Thakkar et al., 2010). For this reason, there is growing interest in developing clean, simple, inexpensive, environmentally friendly methods for the synthesis of nanoparticles. Bacteria, mushrooms, algae and plant extracts can be used in modern alternatives for the production of metal/metal oxide nanoparticles. Green synthesized nanoparticles are associated with organic matter from plant extracts and increase particle stability. Plant-mediated nanoparticles are cheaper compared to microplasm.

In contrast to the time-consuming chemical and physical methods which involve complicated procedures, a green method is much easier and safer to use, and plant-mediated synthesis of nanoparticles is still a new scheme and the outcome is yet to be studied. There are a couple of successful studies in synthesizing iron oxide nanoparticles by using plant extract. For instance, fruit extract of *Artemisia annua* (Basavegowda et al., 2014a), leaf extract of *Perilla frutescens* (Basavegowda et al., 2014b), *Tridax procumbens* (Basavegowda et al., 2014b) and *caricaya papaya* (Latha and Gowri, 2014), peel extract of *plantain* (Venkateswarlu et al., 2013), and also extract of *seaweed K. alvarezii* (Yew et al., 2016).

Different parts of *Juglans regia* (*J. regia*) tree such as kernels, leaves, tree barks and fruit green husks have been utilized in both pharmaceutical and cosmetic industries (Izadiyan et al., 2017; Stampar et al., 2006). A study by Carvalho et al. demonstrated the antioxidant and antimicrobial activities of walnut's leaves, seeds, and green husks (Fernández-Agulló et al., 2013). *J. regia* green husk is one of the major waste products in the industry of walnut production, and little is known about its potential use in any biotechnological application. The findings from Carvalho et al. showed the potential of these

low-cost natural materials to be developed into phenolic compounds for antimicrobial and antiradical applications (Carvalho et al., 2010).

In this research, iron oxide nanoparticles were synthesized with and without the *J. regia* extract to determine the role of extract compounds in size controlling. The non-toxic effect of iron oxide nanoparticles synthesized by *J. regia* extract which hereafter named (*J. regia*/iron oxide nanoparticles) was evaluated in cytotoxicity study. Based on the researcher's knowledge, this is the first attempt to use *J. regia* green husk in green synthesis of iron oxide nanoparticles.

2. Materials and method

Iron (III) chloride hexahydrate ($\text{FeCl}_3 \cdot 6\text{H}_2\text{O}$, 97%) and iron (II) chloride tetrahydrate ($\text{FeCl}_2 \cdot 4\text{H}_2\text{O}$, 99%) were obtained from Sigma-Aldrich (St Louis, MO, USA). Sodium hydroxide (NaOH, 99.0%) was obtained from R&M Chemicals. The *J. regia* green husk was collected from Sorkh-e-Hesar region of Tehran, Iran. All reagents used were of analytical grades. The chemical solutions were prepared in new batches utilizing distilled water, and stored in the dark to prevent photochemical-induced reactions. All glass wares utilized in this study were cleaned with fresh HNO_3/HCl (3:1, v/v), followed by double distilled water (ddH_2O), and dried prior to use. NIH-3 T3 (mouse embryonic fibroblast cell lines) and HT-29 (human colorectal adenocarcinoma cell line) as normal and cancerous cell lines were purchased from Cell Lines Service (ATCC, USA). Dulbecco's Modified Eagle's Medium (DMEM) and trypsin were obtained from Gibco (Invitrogen Corporation, UK). MTT solution was purchased from Sigma.

2.1. Extract preparation

The *J. regia* green husk were washed and dried in an oven at 40 °C for 48 h. The dried green husk was then ground into a mill, stored in glass bottles and kept at room temperature until further analyses. The finely ground *J. regia* green husk (1 g) was added to the 100 mL of the boiling water for 30 min. and then was filtered. The extracts were kept in dark place at 4 °C for future use.

2.2. Synthesis of *J. regia*/iron oxide nanoparticles

To investigate the ability of *J. regia* green husk extract in size control of iron oxide nanoparticles, they prepared via two different methods. At the first, iron oxide nanoparticles were synthesized through co-precipitation method using NaOH. The molar ratio in solution was adjusted to 1:2 by adding a measured amount of Fe^{3+} and Fe^{2+} in 80 mL of deionized water. Then 5 mL of iron solution diluted with 5 mL deionized water and was stirred for 1 h. Then, 2 mL freshly prepared NaOH (2 M) was added to water/ Fe^{3+} - Fe^{2+} suspension under continuous stirring. In the second method, 1 g of *J. regia* was suspended in 100 mL deionized water. Then 5 mL of iron solution diluted with 5 mL of *J. regia* extract and was stirred for 1 hr. Then 2 mL of freshly prepared NaOH (2.0 M) was added to *J. regia*/ Fe^{3+} - Fe^{2+} suspension under continuous stirring. Finally, both suspensions were finally centrifuged, washed three times with distilled water, and dried by oven dryer at 60 °C.

2.3. Characterization

The crystal structure of the nanoparticles was analyzed by powder X-ray diffraction (XRD, Philips, X'pert, Cu Ka), the data of 2θ being typically collected in the range of 10–90°. The magnetic property was measured on a Lakeshore vibrating sample magnetometer (VSM) on the dried samples at room temperature and the sample was measured in powder form. The morphology, nanostructure, particle size and size distribution of the iron oxide nanoparticles were studied by high-resolution transmission electron microscopy (HR-TEM, JEM-2100F). ImageJ (jre-8u91) software were used to measure the nanoparticle size and also the SPSS 20 software for drawing size distribution histogram. The elemental analysis of the *J. regia*/iron oxide nanoparticles, energy dispersion X-ray spectroscopy was carried out on a Shimadzu EDX700HS spectrometer attached to the FESEM. The FTIR spectrum was utilized to recognize the functional groups existing in the synthesized compound. FTIR spectra were recorded over the range of 500–4000 cm^{-1} used the Series 100 FTIR 1650 spectro photometer (PerkinElmer, Waltham, MA, USA). The amount of extract coating the iron oxide nanoparticles was determined by thermogravimetric analysis (TGA) using a TGA Q50 V20 with a 10 °C/min heating rate under a nitrogen atmosphere (10 mL min^{-1}). The measurement was made from 10 °C up to 800 °C. Zeta potential using the Particulate Systems Nano-Plus Zeta/Nano Particle Analyser, Japan, was utilized to measurement the charge of the droplet surface of solution, which may cause effects on the chemical and physical stability of the *J. regia*/iron oxide nanoparticles (Rabinovich-Guilatt et al., 2004).

2.4. Cytotoxicity assay

Cytotoxicity assay measures the killing capacity of test compound against a target cell. One of the common methods to determine cytotoxicity is by MTT (3-[4,5-dimethylthiazol-2-yl]-2,5-diphenyltetrazolium bromide) assay. Mouse embryonic fibroblast cell lines (NIH-3 T3) and human colorectal adenocarcinoma cell line (HT-29) as normal and cancerous cell lines were used in this study. Cultured cells at concentration of 2000 cells/well was prepared and plated (100 $\mu\text{l/well}$) onto 96-well plates. The diluted sample extracts were added to each well with known concentrations; 1, 20, 62.5, 125, 250, 500, and 1000 $\mu\text{g/ml}$. The cells were then incubated for 72 h at 37 °C in a 5% CO_2 incubator. MTT solution was then added to each well and incubated for additional 3 h at 37 °C in the 5% CO_2 incubator. After solubilization of the purple formazan crystals using dimethyl sulfoxide (DMSO), the optical density (OD) of the well was measured using an ELISA reader (Tecan, Sunrise) at a wavelength of 570 nm. The cytotoxicity was recorded as the drug concentration causing 50% growth inhibition of the tumor cells (IC_{50} value) using the formula given below in the Eq. (1) and an inhibition graph was plotted. The images of HT-29 and NIH-3T3 before and after treatment were also assessed by inverted microscope attached to a camera system (Nikon, Eclipse, TS100, EIWD 0.3/OD75).

$$\% \text{ Cell viability} = \frac{\text{OD test sample (mean)}}{\text{OD control (mean)}} \times 100 \quad (1)$$

3. Results and discussion

The *J. regia* green husk suspension was pale yellow, which turned to dark color after the addition of the Fe^{+3} and Fe^{+2} to the *J. regia* green husk suspension and addition of NaOH solution as a reducing agent (Fig. 1).

The possible chemical equations for preparing of *J. regia*/iron oxide nanoparticles was shown in Eqs. (2) and (3): The overall reaction may be written as follows (Hribernik et al., 2012; Shameli, 2013).

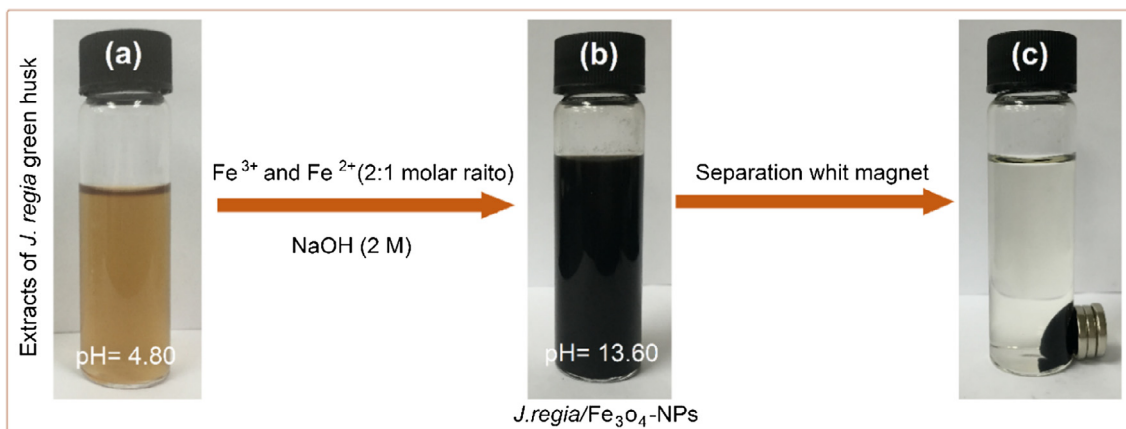
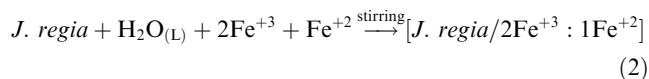


Fig. 1 (a) *J. regia* extracts, (b) *J. regia*/iron oxide nanoparticles and (c) separation of synthesized *J. regia*/iron oxide nanoparticles from the reaction mixture using an external magnet.

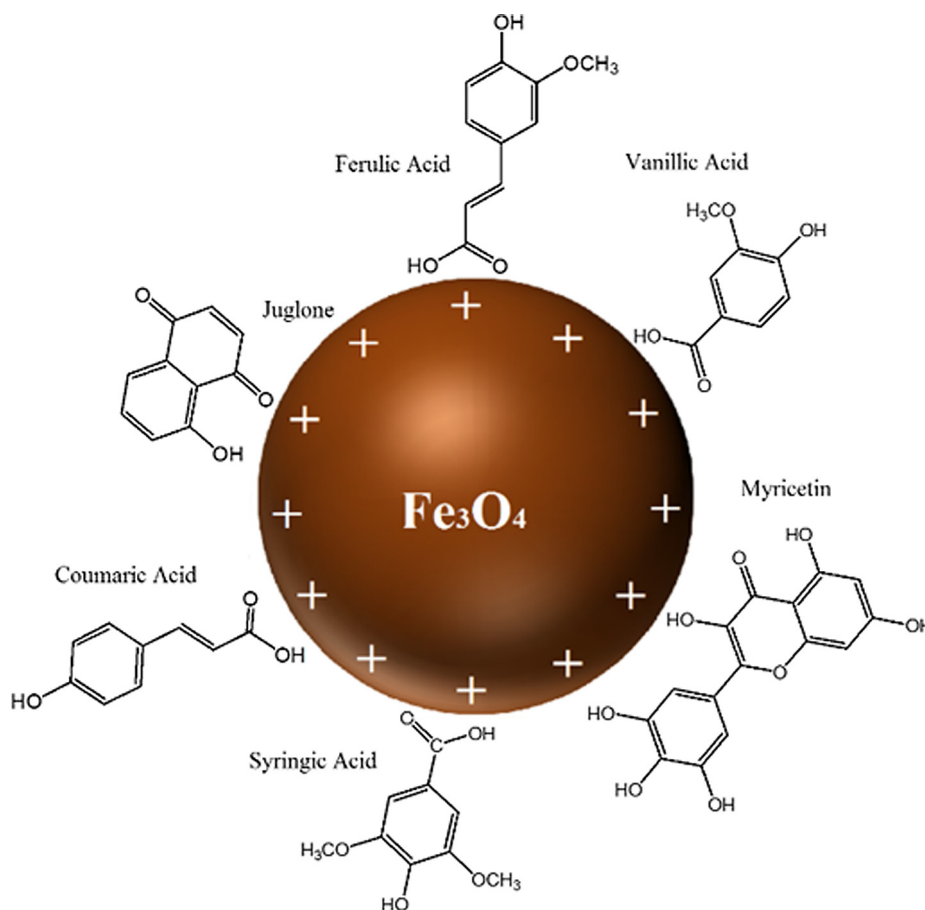
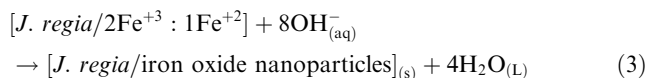


Fig. 2 Schematic of synthesized *J. regia*/iron oxide nanoparticles interactions with activated functional groups of *J. regia*.



According to Cosmulescu et al. findings, the *J. regia* has various types of phenols compounds. The high-performance liquid chromatography technique utilized in identification of six phenolic compounds in green husk extract including vanillic acid, myricetin, coumaric acid, syringic acid, juglone, and ferulic acid (Cosmulescu et al., 2010). All the phenolic compounds in *J. regia* extract are presented in Fig. 2. According to this schematic illustration that we suggested, they could be involved closely in the stabilization of iron oxide nanoparticles where the presence of electrons from oxygen atoms helped in the absorption of compounds on *J. regia*/iron oxide nanoparticles surface.

3.1. X-Ray diffraction analysis

The XRD spectrum of *J. regia* green husk extract represents in Fig. 3 there is no obvious peaks due to the absence of *J. regia*/iron oxide nanoparticles. A broad diffraction peak was represented in Fig. 3a at 28.42°, which is attributed to *J. regia* green husk. The decreasing in intensity or shifting the peak suggested that the *J. regia*/iron oxide nanoparticles have interaction with biomolecules present in the extract. However, Fig. 3b demonstrates intense peaks at the 2θ values of 30.30, 35.68, 43.45, 53.83, 57.42, 62.93, and 74.58 which correspond to the (2 0 0), (3 1 1), (4 0 0), (4 2 2), (5 1 1), (4 4 0), and (5 3 3) crystallographic planes proving the structure of *J. regia*/iron oxide nanoparticles to be cubic structure (Ref. No. 01-075-0449). The crystallite size of synthesized *J. regia*/iron oxide nanopar-

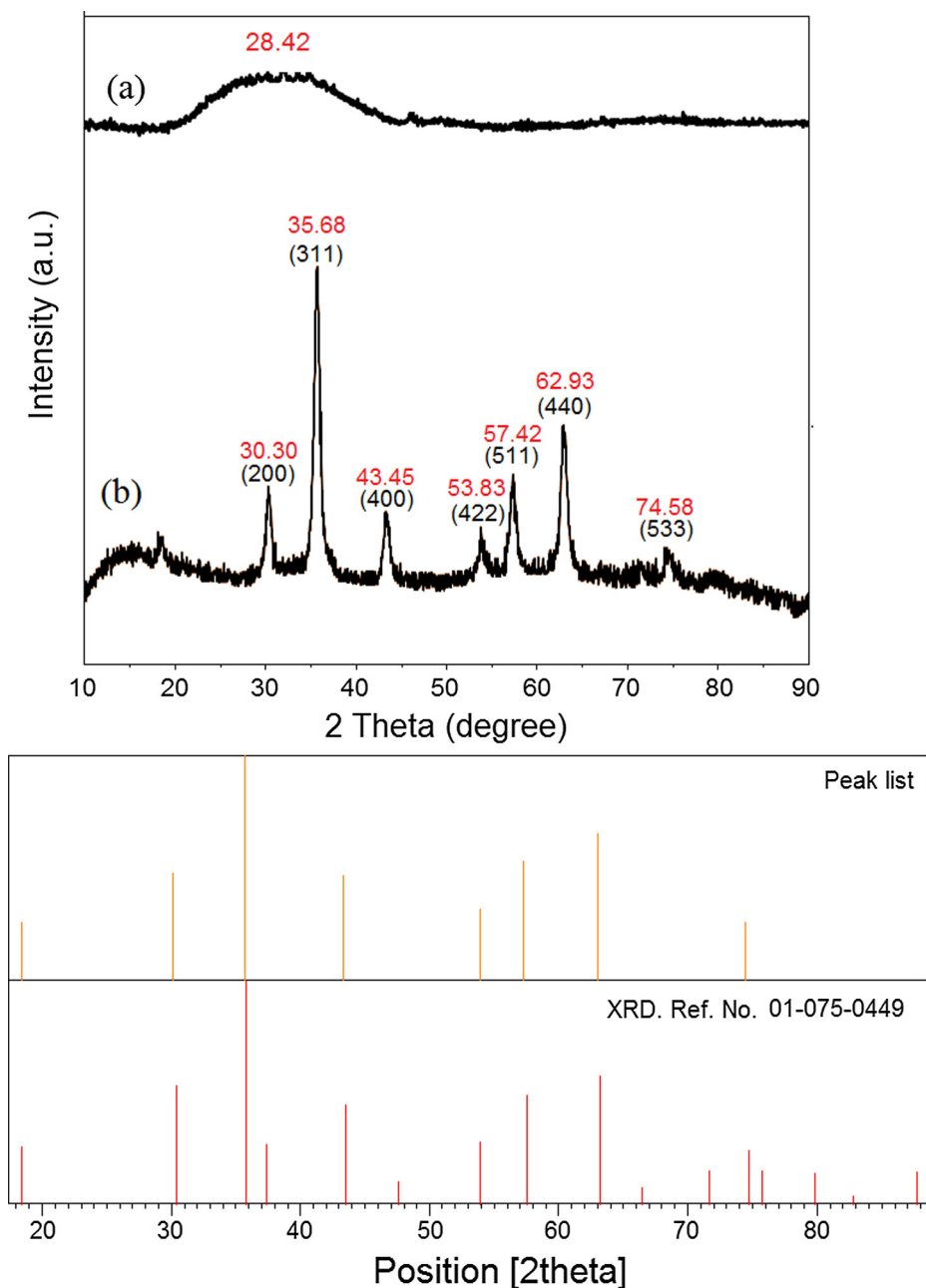


Fig. 3 the XRD of *J. regia* (a) and *J. regia*/iron oxide nanoparticles (b).

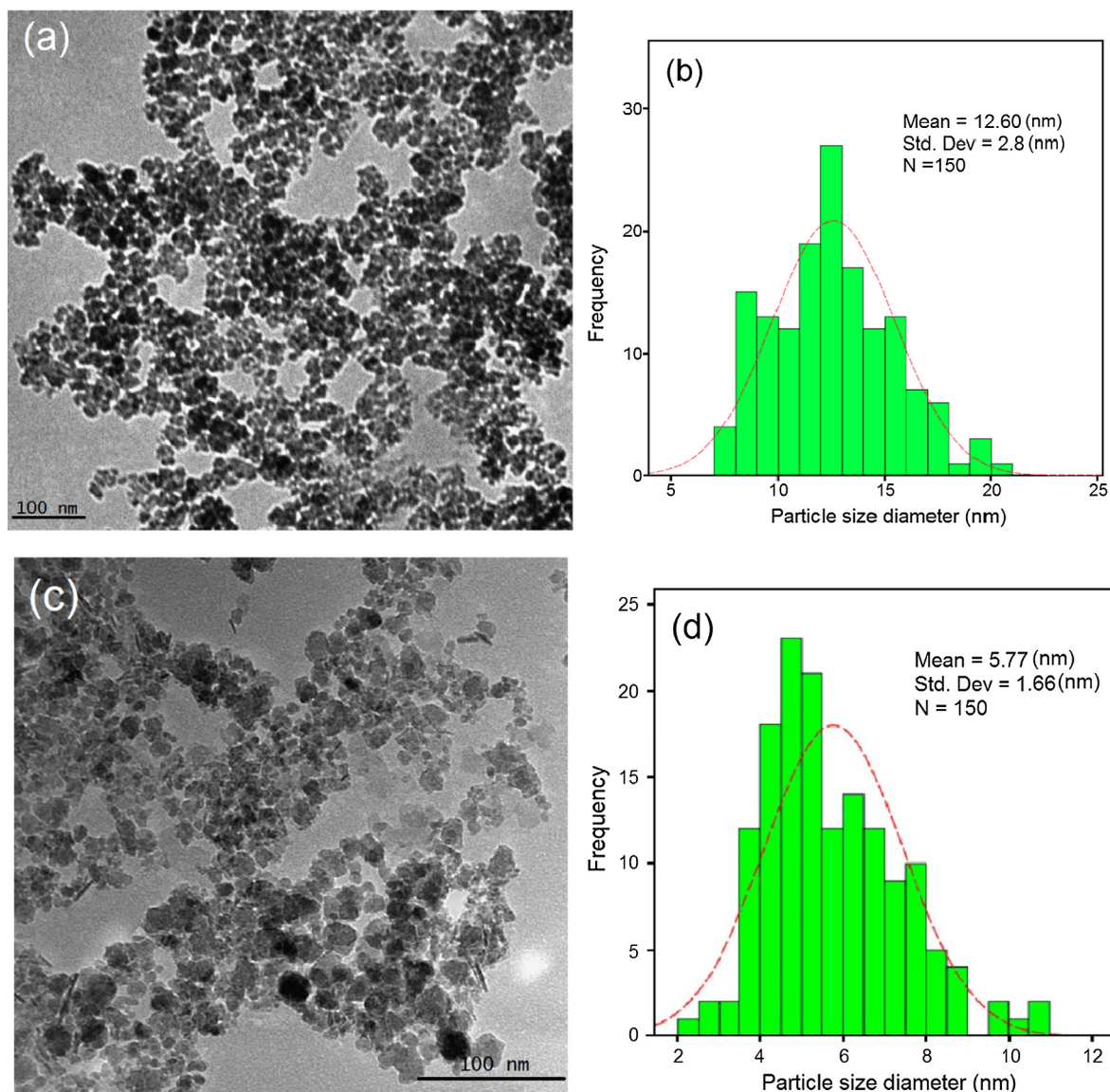


Fig. 4 HR-TEM images (a), particle size distribution histogram of iron oxide nanoparticles (b), HR-TEM images (c) and particle size distribution histogram of *J. regia*/iron oxide nanoparticles (d).

ticles can be calculated using the Debye-Scherrer equation (Raman and Doble, 2014), which reveals a relationship between X-ray diffraction peak broadening and crystallite size. The Debye-Scherrer equation is shown in Eq. (4):

$$d = \frac{k\lambda}{\beta \cos \theta} \quad (4)$$

where d is the average crystallite size of synthesized *J. regia*/iron oxide nanoparticles, K is the Scherrer constant with a value from 0.9 to 1, λ is the X-ray wavelength (0.154 nm), β is the line broadening in radians, and θ is the Bragg angle. Using the equation, the estimated crystallite mean size of synthesized *J. regia*/iron oxide nanoparticles was 10.30 nm, which was calculated from the full-width of the *J. regia*/iron oxide nanoparticles diffraction peak (Sá et al., 2014) at all 2θ . Based on the X-ray diffraction pattern, the synthesized *J. regia*/iron oxide nanoparticles were figured out to be high purity crystalline, as no impurity peak was observed.

3.2. Morphological study

Fig. 4 illustrates the HR-TEM images of synthesized *J. regia*/iron oxide nanoparticles through co-precipitation method using NaOH and using *J. regia*. Fig. 4a demonstrates the agglomeration of *J. regia*/iron oxide nanoparticles and also shows that a majority of the nanoparticles are in cubic shape. The particle size distribution histogram was designed based on the counted 150 nanoparticles'. The mean size of the particle is 12.60 nm with 2.87 nm standard deviation. Fig. 4d shows the mean size of the particle is 5.77 nm with 1.66 nm standard deviation, moreover the agglomeration is reduced obviously and particles with smaller size have fabricated. Based on the Debye-Scherrer equation the crystallite size of the synthesized *J. regia*/iron oxide nanoparticles was found to be 1.89 nm from XRD analysis, which is in an agreement with the result obtained from the HR-TEM and also the cubic structure of nanoparticles. By comparison between HR-TEM images, it

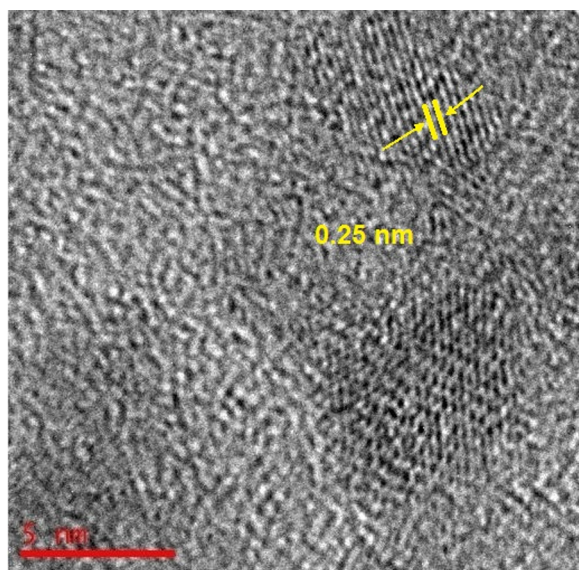
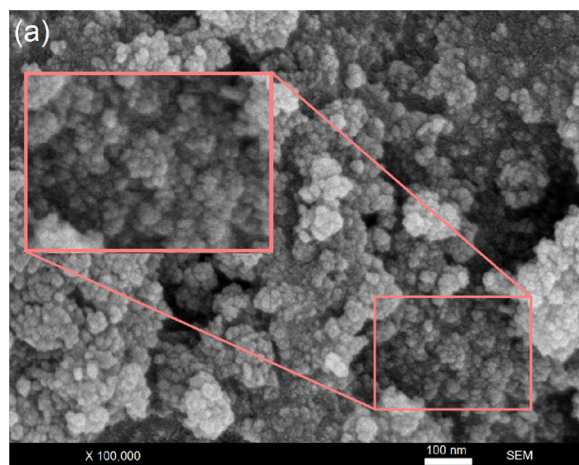


Fig. 5 The electron diffraction pattern of *J. regia*/iron oxide nanoparticles by using the HR-TEM image.

can result that the extract had a significant influence on the size of nanoparticles and played the main role in control size process.

The electron diffraction pattern of *J. regia*/iron oxide nanoparticles by using HR-TEM image was shown in Fig. 5. The electron diffraction pattern and HR-TEM image confirm that *J. regia*/iron oxide nanoparticles have good and regular crystallinity. The lattice spacing measured on the HR-TEM image was 0.25 nm. The values of d spacing between the lattice of Fe particles are in good agreement with those reported in the literature for iron oxide nanoparticles (3 1 1), which further supported the metallic state of the supported iron oxide nanoparticles (Sisodiya et al., 2015).

Fig. 6 depicts the distribution size and identification of the iron elements using by FESEM image and EDX. FESEM image supports the HR-TEM results that the *J. regia*/iron oxide nanoparticles have small size (Fig. 6a). Each element has a unique atomic structure, EDX provides information



about the chemical composition of the compound. EDX is an interaction between X-rays and the compound being investigated. Therefore, when this analysis is carried out, the X-rays that are reflected off the compound give peaks. The amplitude of the peaks obtained help to identify the elements present in the compound being studied. The peak amplitude of iron starts from 0.7 to 7 keV. Fig. 6b confirms the presence of the iron elements in the compounds using EDX. The results also demonstrate the high percentage of iron present in the particles. The EDX spectra revealed the presence of iron peaks in three different areas (0.7, 6.4 and 7.0).

3.3. Zeta potential analysis

The zeta potential analysis was carried out to gather information about the surface properties of the nanoparticles. This equipment is able to reveal the stability of particular systems in the long-term. A zeta value of about ± 30 mV is needed for a physical suspension stabilized by the repulsion of the electrostatic role. Additionally, when combined electrostatic as well as steric stabilization electrostatic and steric stabilization, ± 20 mV is sufficient (Şen and Erboz, 2010). Zeta potential results have a negative value for *J. regia* and *J. regia*/iron oxide nanoparticles prepared at room temperature. The zeta potential of *J. regia* has a -28.68 mV value, whereas the *J. regia*/iron oxide nanoparticles values, changed to -26.90 mV [Fig. 7(a and b)]. Based on the sufficient value for the stability of the solution, the *J. regia*/iron oxide nanoparticles showed sufficient stability. The zeta potential of the *J. regia*/iron oxide nanoparticles is slowly reduced, however, not less than the sufficient amount for stable expression, thereby producing stable *J. regia*/iron oxide nanoparticles.

Also we studied the pH effect on the synthesis process of iron oxide nanoparticle. The initial pH of extract was 2 the NaOH (2M) solution was added drop wise sample and till pH 10 no iron oxide nanoparticle was observed but in pH 11–14 iron oxide nanoparticles migrate onto magnet.

3.4. Vibrating sample magnetometer

The vibrating sample magnetometer (VSM) was applied to test the magnetic properties of *J. regia*/iron oxide nanoparticles.

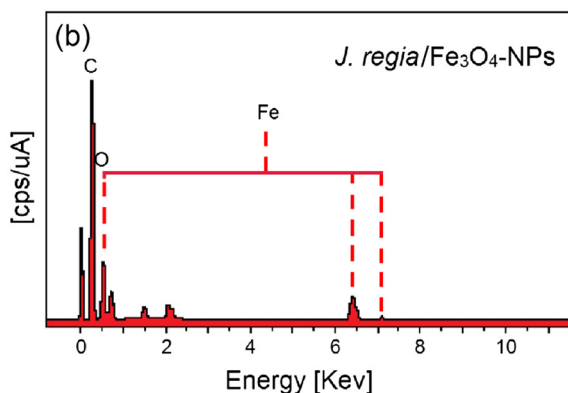


Fig. 6 FESEM micrographs (a) and EDX spectra of the *J. regia*/iron oxide nanoparticles (b).

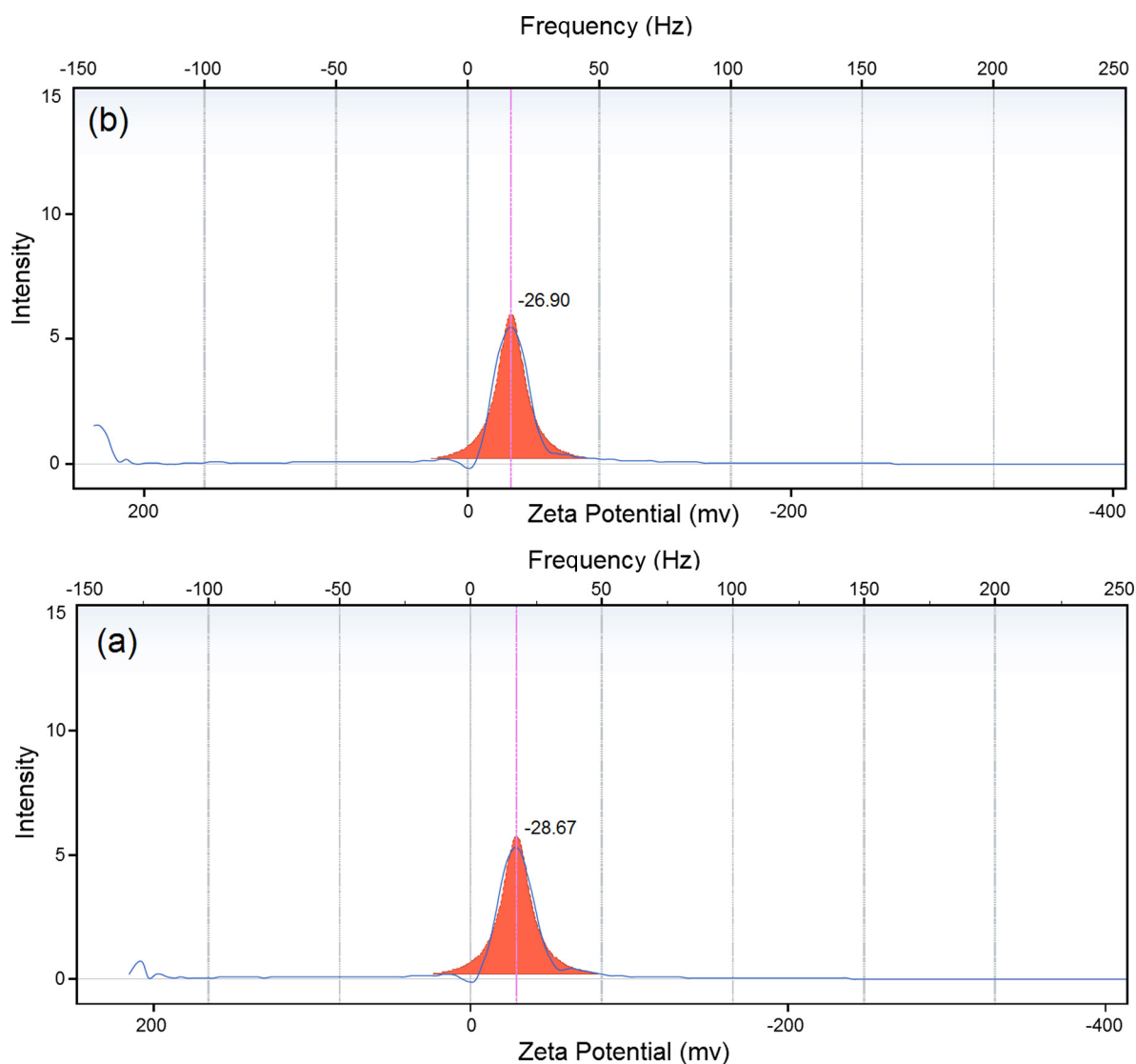


Fig. 7 Zeta potential results for *J. regia* (a) and *J. regia*/iron oxide nanoparticles (b).

Magnetic characterization of the *J. regia*/iron oxide nanoparticles (1.0 g) at room temperature is represented in Fig. 8. It can be seen from the magnetization curves that high saturation magnetization (Ms) of the *J. regia*/iron oxide nanoparticles $53.32 \text{ emu}\cdot\text{g}^{-1}$ with low coercivity 32.50 Oe were obtained. According to the magnetization curves, the *J. regia*/iron oxide nanoparticles has high saturation magnetization (Ms) it would be due to more iron oxide nanoparticles trapped in the *J. regia* substance. The lag or delay of magnetic materials is commonly termed as magnetic hysteresis, relates to the magnetization properties of a material by which it firstly becomes magnetized and then demagnetized. Hysteresis measurements of *J. regia*/iron oxide nanoparticles were performed by an Automatic Magnetic Hysteresis graph for a magnetic field ranging from -50 Oe to $+50 \text{ Oe}$ are shown in Fig. 8b. Using the hysteresis loop presented in Fig. 8b, the hysteresis parameters viz. coercivity (Hc), are estimated 32.50 Oe. Fig. 8c clearly shows the synthesized *J. regia*/iron oxide nanoparticles are able to be rapidly attracted by an external permanent magnet, which demonstrates that the *J. regia*/iron oxide nanoparticles have

magnetic properties. After the magnet was removed, the *J. regia*/iron oxide nanoparticles were easily dispersed by shaking.

3.5. Fourier transform infrared spectroscopy study

The FT-IR spectra of *J. regia* and *J. regia*/iron oxide nanoparticles are demonstrated in Fig. 9. Based on the FT-IR spectrum of *J. regia* (Fig. 9a), the absorption peaks at 3405 cm^{-1} are assigned to vibrations of stretching of the groups of $-\text{OH}$ and the $2960\text{--}2850 \text{ cm}^{-1}$ region reflects the C-H stretch, accordingly (Chen et al., 2011). The intense at 1596 cm^{-1} band is utilized for C=C vibrations of stretching (Qin et al., 2011). The 1400 cm^{-1} peak is utilized for the C=C stretch for aromatic vibrations (Chen et al., 2011). The 1117 cm^{-1} peak reflects the C-O stretch and deformation bands of in the lignin (Sun et al., 2005). The iron oxide nanoparticles presence in the *J. regia*'s substrate is proven by the bands of adsorption at approximately $295\text{--}538 \text{ cm}^{-1}$ which reaffirm the stretching of the Fe-O as observed in Fig. 9b (Karaoğlu et al., 2011).

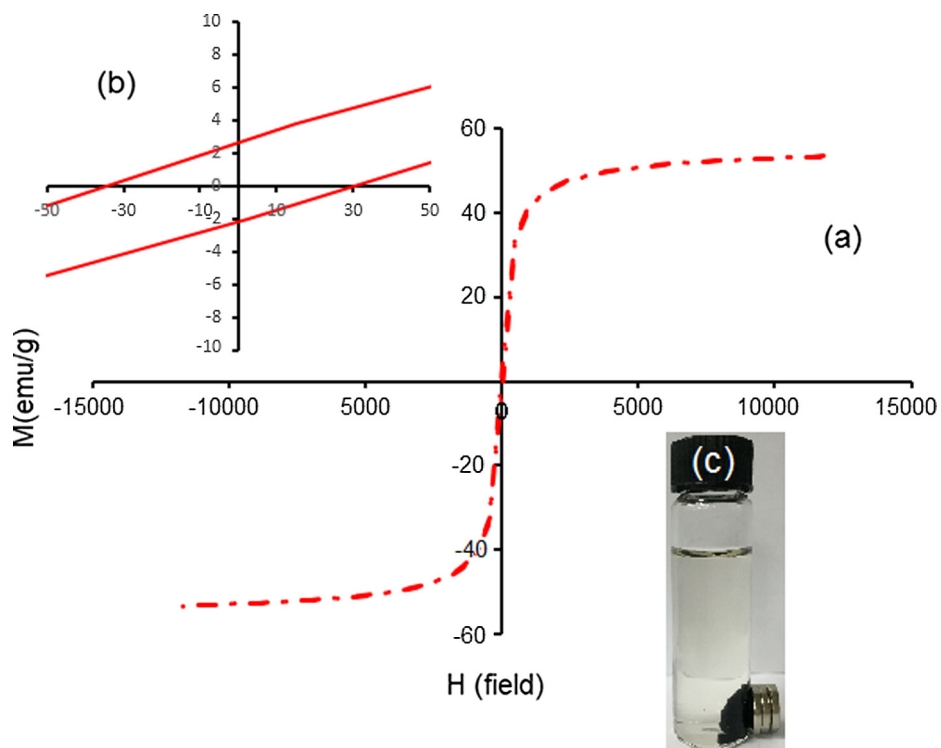


Fig. 8 Vibrating sample magnetometer plots of *J. regia*/iron oxide nanoparticles coated with *J. regia* (a), hysteresis loop of *J. regia*/iron oxide nanoparticles (b) and (c) separation of synthesizing *J. regia*/iron oxide nanoparticles.

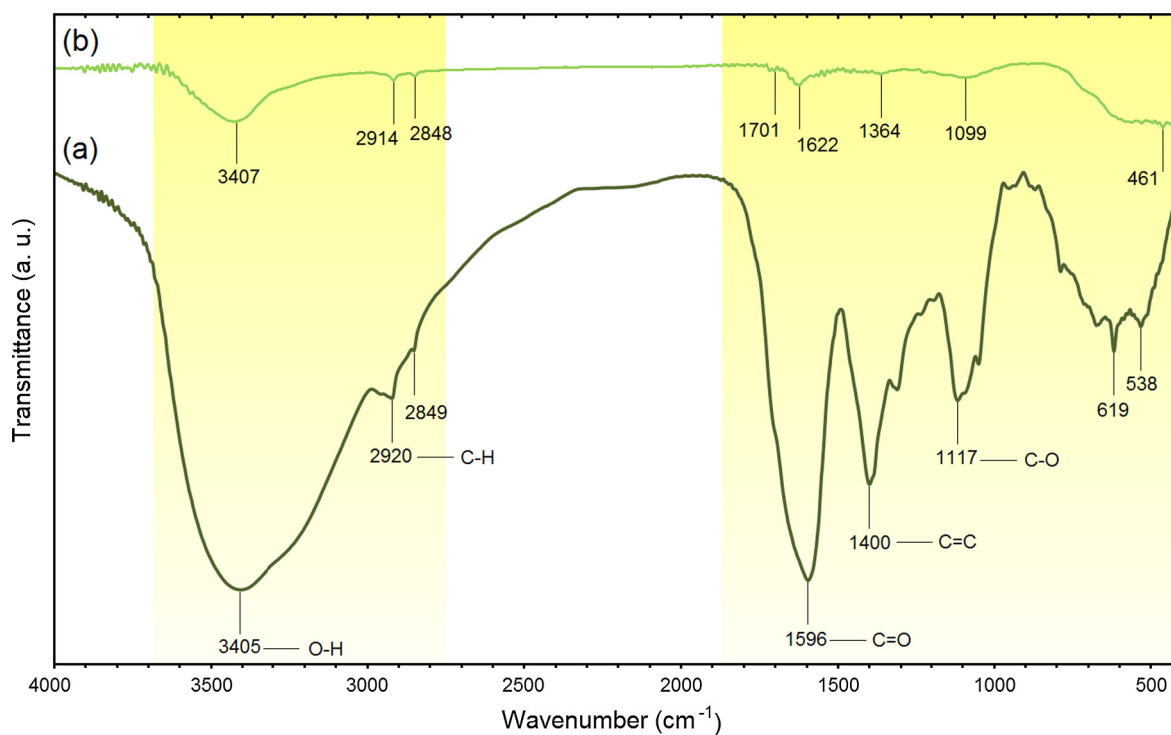


Fig. 9 FTIR spectra for *J. regia* (a) and *J. regia*/iron oxide nanoparticles (b).

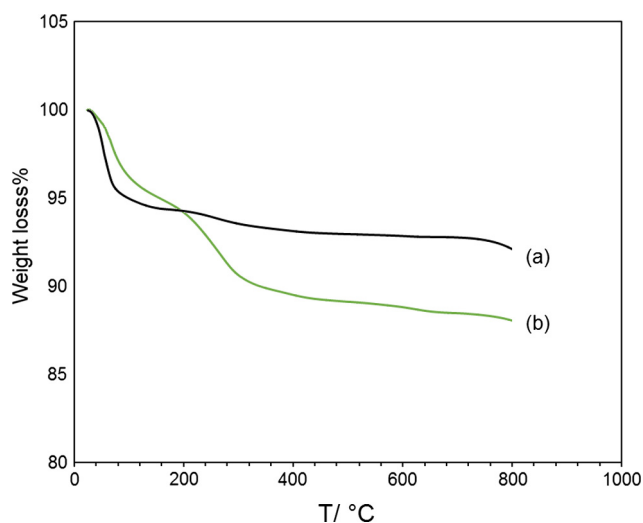


Fig. 10 Weight loss of magnetic particles coated with *J. regia*, the thermogram of pure iron oxide nanoparticles (a) and *J. regia*/iron oxide nanoparticles has been included.

The bands at 1622 cm^{-1} reveal reactions between the groups of hydroxyl on the *J. regia*/iron oxide nanoparticles surface as well as the *J. regia* groups of carboxylate (Zhao et al., 2010). The peaks of *J. regia*/iron oxide nanoparticles in comparison with peaks of *J. regia* reveals a reduction in the adsorption peaks' intensity; which is due to the partial reduction of the *J. regia* (Chang et al., 2012). A small shifting occurred in peaks such as 2920–2914, 1596–1622, 1400–1364 and 1117–1099, and changes in intensity of all peaks, suggesting the mineral composition creation. This outcome shows that the *J. regia* could be coated on the iron oxide nanoparticles in a successful manner.

3.6. Thermogravimetric analysis

Both TGA curves show a slight loss of weight in the temperature range of 30–100 °C due to the moisture content in the sample. As shown in Fig. 10a from 100 to 800 °C transformation of Fe_3O_4 to $\gamma\text{-Fe}_2\text{O}_3$ and Fe_2O_3 to $\alpha\text{-Fe}_2\text{O}_3$ were happened. In Fig. 10b the mass profile exhibited a well-defined decrease over a temperature range of 100–340 °C. This weight loss was due to desorption and subsequent evaporation of *J. regia*. Based on the Fig. 10b from 340 to 800 °C transformation of Fe_3O_4 to $\alpha\text{-Fe}_2\text{O}_3$ were obtained (García-Jimeno and Estelrich, 2013). According the result the final weight loss of pure iron oxide nanoparticle and *J. regia*/iron oxide nanoparticle are 92.85% and 88.03%, respectively, then, 4.82% of weight loss is due to evaporation of *J. regia*.

3.7. In vitro cytotoxicity assay

As shown in Fig. 11, the cytotoxicity effects of the synthesized *J. regia*/iron oxide nanoparticles were investigated on 3T3 (Mouse Embryonic fibroblast cell lines) and HT-29 (human colorectal adenocarcinoma cell line, estrogen receptor negative) cell lines as normal and cancerous cell lines, respectively. The cells were treated with the *J. regia*/iron oxide nanoparticles at various concentrations (1–1000 $\mu\text{g/ml}$) incubated at 37 °C for 72 h. The prepared *J. regia* green husk-coated *J. regia*/iron oxide nanoparticles also demonstrated no significant toxicity even in concentrations up to 1000 $\mu\text{g/ml}$ on normal cell lines in the resazurin reduction assay, meaning that the *J. regia*/iron oxide nanoparticles are well tolerated by 3T3 cells (Fig. 11a). Green husk coated *J. regia*/iron oxide nanoparticles had no toxic effect on cancerous (HT-29; 1000 $\mu\text{g/ml}$) cell lines in higher concentrations (Fig. 11b). Hence, the IC_{50} was not determined for normal and cancerous cell lines. These results

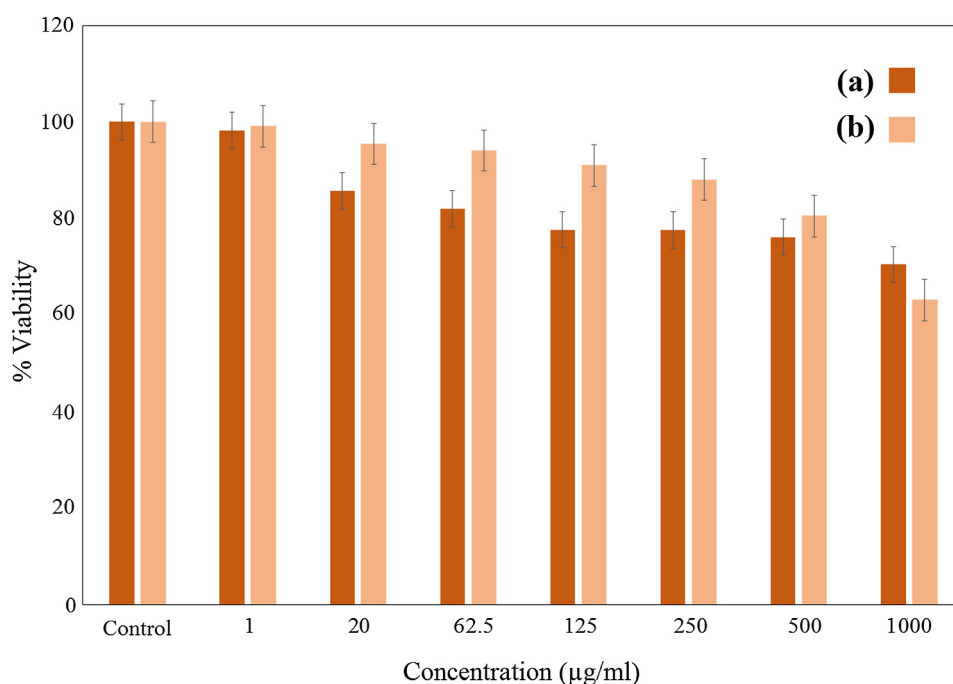


Fig. 11 MTT assays of (a) normal human fibroblast (3T3) cell line, and anticancer activity in (b) (human colorectal adenocarcinoma (HT-29) cell lines after 72 h of treatment with *J. regia*/iron oxide nanoparticles.

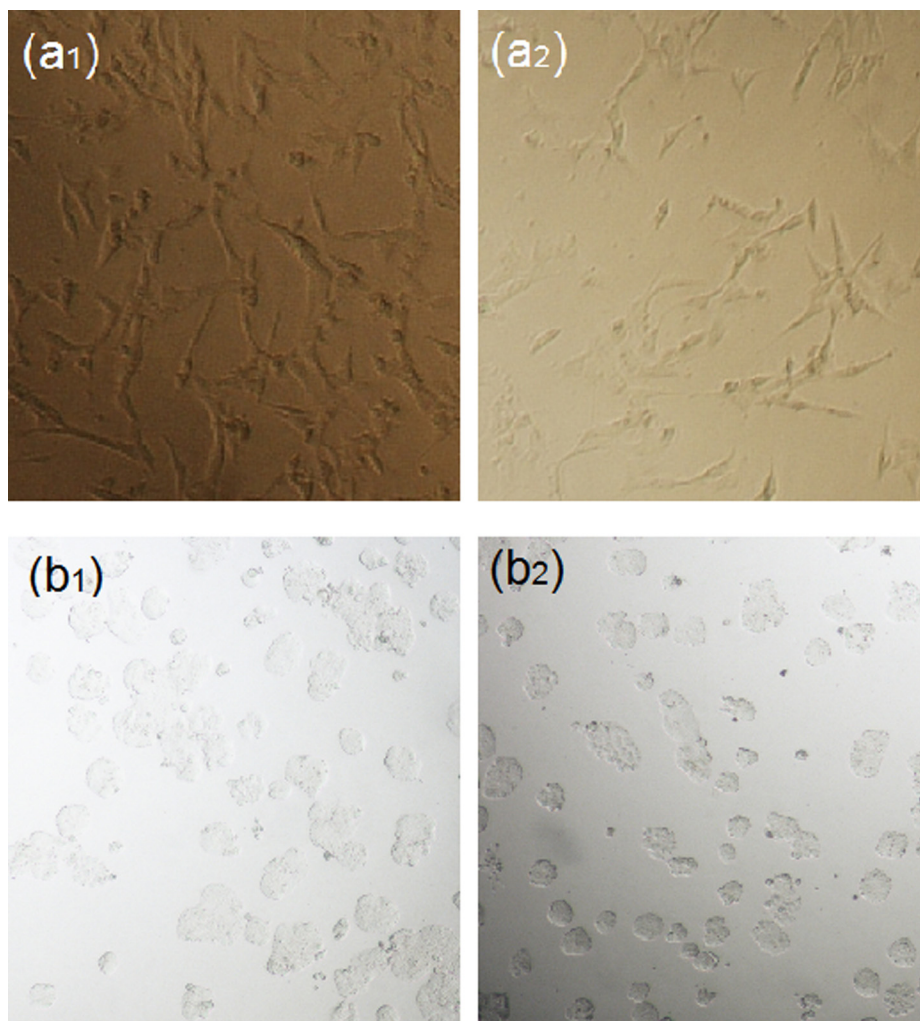


Fig. 12 Microscopic images of *J. regia*/iron oxide nanoparticles on 3T3 (control a₁ and treated cell a₂) and HT-29 (control b₁ and treated cell b₂) respectively.

are demonstrated the possibility of these *J. regia*/iron oxide nanoparticles for different biomedical applications. In a previous study, the bio-functional starch/iron oxide nanoparticles have non-toxic effects on normal and cancerous cervical cell lines, making them suitable candidates for various biological applications (Gholoobi et al., 2017).

Fig. 12(a₁ and b₁) shows images of cell lines in the absence of *J. regia*/iron oxide nanoparticles. As shown, the cells are neatly connected with each other with a high concentration of cells in the cell lines. Fig. 12(a₂ and b₂) represents images in the presence of *J. regia*/iron oxide nanoparticles, bilayers of extract capped nanoparticles interact with membrane proteins and disrupt the signaling process with the result that some of the cells were dying and also cell concentration is less than before.

4. Conclusion

The *J. regia*/iron oxide nanoparticles were synthesized using *J. regia* green husk as a control size. According to the HR-TEM the *J. regia*/iron oxide nanoparticles were prepared for the first

time in cubic structure and the average size of them was 5.77 ± 1.66 nm. The crystallite of the synthesized *J. regia*/iron oxide nanoparticles was found from XRD analysis, which is in an agreement with the result obtained from the HR-TEM and also has strong magnetic properties were observe form VSM. The FT-IR results of the nanoparticles were shown that *J. regia* was successfully coted in iron oxide nanoparticles which is confirm by TGA. This method is inexpensive and environmentally friendly leading to the preparation of very small iron oxide nanoparticles. Moreover, the *J. regia*/iron oxide nanoparticles have non-toxic effects on normal and cancerous cervical cell lines, making them suitable candidates for various biological applications. In comparison to iron oxide, *J. regia*/iron oxide nanoparticles show higher magnetic properties and it would be more effective for drug targeting in further study.

Acknowledgments

This research was funded by the Ministry of Education, Malaysia [grant number R.K130000.7843 # 4F793 under

FRGS and Q.K130000.2543. # 17H60 under Tier 1 grants]. The authors also would like to thank the Research Management Centre (RMC), UTM for the conducive research environment.

References

- Abdullah, N.H., Shameli, K., Abdullah, E.C., Abdullah, L.C., 2017. A facile and green synthetic approach toward fabrication of starch-stabilized magnetite nanoparticles. *Chin. Chem. Lett.* 28, 1590–1596.
- Abedini, A., Daud, A.R., Hamid, M.A.A., Othman, N.K., 2014. Radiolytic formation of Fe₃O₄ nanoparticles: influence of radiation dose on structure and magnetic properties. *PLoS One* 9, 90055.
- Bagheri, S., Chandrappa, K., Hamid, S.B.A., 2013. Generation of hematite nanoparticles via sol-gel method. *Res. J. Chem. Sci.* 3, 62–68.
- Basavegowda, N., Magar, K.B.S., Mishra, K., Lee, Y.R., 2014a. Green fabrication of ferromagnetic Fe₃O₄ nanoparticles and their novel catalytic applications for the synthesis of biologically interesting benzoxazinone and benzthioxazinone derivatives. *New J. Chem.* 38, 5415–5420.
- Basavegowda, N., Mishra, K., Lee, Y.R., 2014b. Sonochemically synthesized ferromagnetic Fe₃O₄ nanoparticles as a recyclable catalyst for the preparation of pyrrolo[3,4-c]quinoline-1,3-dione derivatives. *RSC Adv.* 4, 61660–61666.
- Benelli, G., 2016a. Plant-mediated biosynthesis of nanoparticles as an emerging tool against mosquitoes of medical and veterinary importance: a review. *Parasitol. Res.* 115, 23–34.
- Benelli, G., 2016b. Plant-mediated synthesis of nanoparticles: a newer and safer tool against mosquito-borne diseases. *Asian Pac. J. Trop. Biomed.* 4, 353–354.
- Benelli, G., Iacono, A.L., Canale, A., Mehlhorn, H., 2016. Mosquito vectors and the spread of cancer: an overlooked connection. *Parasitol. Res.* 115, 2131–2137.
- Bomati-Miguel, O., Mazeina, L., Navrotsky, A., Veintemillas-Verdaguer, S., 2008. Calorimetric study of maghemite nanoparticles synthesized by laser-induced pyrolysis. *Chem. Mater.* 20, 591–598.
- Burtea, C., Laurent, S., Roch, A., Vander Elst, L., Muller, R.N., 2005. C-MALISA (cellular magnetic-linked immunosorbent assay), a new application of cellular ELISA for MRI. *J. Inorg. Biochem.* 99, 1135–1144.
- Carenza, E., Barceló, V., Morancho, A., Montaner, J., Rosell, A., Roig, A., 2014. Rapid synthesis of water-dispersible superparamagnetic iron oxide nanoparticles by a microwave-assisted route for safe labeling of endothelial progenitor cells. *Acta Biomater.* 10, 3775–3785.
- Carvalho, M., Ferreira, P.J., Mendes, V.S., Silva, R., Pereira, J.A., Jerónimo, C., Silva, B.M., 2010. Human cancer cell antiproliferative and antioxidant activities of *Juglans regia* L. *Food Chem. Toxicol.* 48, 441–447.
- Chang, Y.-P., Ren, C.-L., Qu, J.-C., Chen, X.-G., 2012. Preparation and characterization of Fe₃O₄/graphene nanocomposite and investigation of its adsorption performance for aniline and p-chloroaniline. *Appl. Surf. Sci.* 261, 504–509.
- Chen, X., Yu, J., Zhang, Z., Lu, C., 2011. Study on structure and thermal stability properties of cellulose fibers from rice straw. *Carbohydr. Polym.* 85, 245–250.
- Chourpa, I., Douzic-Eyrolles, L., Ngaboni-Okassa, L., Fouquet, J.-F., Cohen-Jonathan, S., Soucé, M., Marchais, H., Dubois, P., 2005. Molecular composition of iron oxide nanoparticles, precursors for magnetic drug targeting, as characterized by confocal Raman microspectroscopy. *Analyst* 130, 1395–1403.
- Cosmulescu, S.N., Trandafir, I., Achim, G., Mihai, B., Baciua, A., Gruia, M., 2010. Phenolics of green husk in mature walnut fruits. *Not. Bot. Horti Agrobot Cluj Napoca* 38, 53.
- Darezeshki, E., Ranjbar, M., Bakhtiari, F., 2010. One-step synthesis of maghemite (γ -Fe₂O₃) nano-particles by wet chemical method. *J. Alloy Compd.* 502, 257–260.
- Dinesh, D., Murugan, K., Madhiyazhagan, P., Panneerselvam, C., Kumar, P.M., Nicoletti, M., Jiang, W., Benelli, G., Chandramohan, B., Suresh, U., 2015. Mosquitocidal and antibacterial activity of green-synthesized silver nanoparticles from *Aloe vera* extracts: towards an effective tool against the malaria vector *Anopheles stephensi*. *Parasitol. Res.* 114, 1519–1529.
- Fernández-Agulló, A., Pereira, E., Freire, M., Valentao, P., Andrade, P., González-Álvarez, J., Pereira, J., 2013. Influence of solvent on the antioxidant and antimicrobial properties of walnut (*Juglans regia* L.) green husk extracts. *Ind. Crop Prod.* 42, 126–132.
- García-Jimeno, S., Estelrich, J., 2013. Ferrofluid based on polyethylene glycol-coated iron oxide nanoparticles: characterization and properties. *Colloids Surf. A: Physicochem. Eng. Aspects* 420, 74–81.
- Gholoobi, A., Meshkat, Z., Abnous, K., Ghayour-Mobarhan, M., Ramezani, M., Shandiz, F.H., Verma, K., Darroudi, M., 2017. Biopolymer-mediated synthesis of Fe₃O₄ nanoparticles and investigation of their in vitro cytotoxicity effects. *J. Mol. Struct.* 1141, 594–599.
- Giri, S., Samanta, S., Maji, S., Ganguli, S., Bhaumik, A., 2005. Magnetic properties of α -Fe₂O₃ nanoparticle synthesized by a new hydrothermal method. *J. Magn. Magn. Mater.* 285, 296–302.
- Govindarajan, M., Benelli, G., 2017. A facile one-pot synthesis of eco-friendly nanoparticles using carissacarandas: ovicidal and larvicidal potential on malaria, dengue and filariasis mosquito vectors. *J. Cluster Sci.* 28, 15–36.
- Govindarajan, M., Nicoletti, M., Benelli, G., 2016. Bio-physical characterization of poly-dispersed silver nanocrystals fabricated using *Carissa spinarum*: a potent tool against mosquito vectors. *J. Cluster Sci.* 27, 745–761.
- Gupta, A.K., Gupta, M., 2005. Synthesis and surface engineering of iron oxide nanoparticles for biomedical applications. *Biomaterials* 26, 3995–4021.
- Hribernik, S., Sfiligoj-Smole, M., Bele, M., Gyergyek, S., Jamnik, J., Stana-Kleinschek, K., 2012. Synthesis of magnetic iron oxide particles: Development of an in situ coating procedure for fibrous materials. *Colloids Surf. A: Physicochem. Eng. Aspects* 400, 58–66.
- Huang, J., Cao, Y., Shao, Q., Peng, X., Guo, Z., 2017. Magnetic nanocarbon adsorbents with enhanced hexavalent chromium removal: morphology dependence of fibrillar vs particulate structures. *Ind. Eng. Chem. Res.* 56, 10689–10701.
- Istudor, V., 2004. Pharmacologically active natural compounds for lung cancer. *Altern. Med. Rev.* 9, 402–419.
- Izadiyan, Z., Shameli, K., Hara, H., Taib, S.H.M., 2017. Cytotoxicity assay of biosynthesis gold nanoparticles mediated by walnut (*Juglans regia*) green husk extract. *J. Mol. Struct.* 151, 97–105.
- Kalantari, K., Ahmad, M.B., Masoumi, H.R.F., Shameli, K., Basri, M., Khandanlou, R., 2015. Rapid and high capacity adsorption of heavy metals by Fe₃O₄/montmorillonite nanocomposite using response surface methodology: preparation, characterization, optimization, equilibrium isotherms, and adsorption kinetics study. *J. Taiwan Inst. Chem. Eng.* 49, 192–198.
- Karaoğlu, E., Baykal, A., Erdem, H., Alpsoy, L., Sozeri, H., 2011. Synthesis and characterization of dl-thioctic acid (DLTA)-Fe₃O₄ nanocomposite. *J. Alloy Compd.* 509, 9218–9225.
- Kim, J.-H., Tratnyek, P.G., Chang, Y.-S., 2008. Rapid dechlorination of polychlorinated dibenzo-p-dioxins by bimetallic and nanosized zerovalent iron. *Environ. Sci. Technol.* 42, 4106–4112.
- Kuppusamy, P., Yusoff, M.M., Maniam, G.P., Govindan, N., 2016. Biosynthesis of metallic nanoparticles using plant derivatives and their new avenues in pharmacological applications—an updated report. *Saudi Pharm. J.* 24, 473–484.
- Latha, N., Gowri, M., 2014. Bio Synthesis and characterisation of Fe₃O₄ nanoparticles using caricaya papaya leaves extract. *IJSR NET* 12, 17.

- Liu, T., Yu, K., Gao, L., Chen, H., Wang, N., Hao, L., Li, T., He, H., Guo, Z., 2017. A graphene quantum dot decorated SrRuO₃ mesoporous film as an efficient counter electrode for high-performance dye-sensitized solar cells. *J. Mater. Chem. A* 5, 17848–17855.
- Lou, X., Lin, C., Luo, Q., Zhao, J., Wang, B., Li, J., Shao, Q., Guo, X., Wang, N., Guo, Z., 2017. Crystal structure modification enhanced FeNb₁₁O₂₉ anodes for lithium-ion batteries. *Chem. Electro Chem.* 4, 3171–3180.
- Murugan, K., Aarathi, N., Kovendan, K., Panneerselvam, C., Chandramohan, B., Kumar, P.M., Amerasan, D., Paulpandi, M., Chandirasekar, R., Dinesh, D., 2015. Mosquitocidal and antiplasmodial activity of *Senna occidentalis* (Cassiae) and *Ocimum basilicum* (Lamiaceae) from Maruthamalai hills against *Anopheles stephensi* and *Plasmodium falciparum*. *Parasitol. Res.* 114, 3657–3664.
- Pardoe, H., Clark, P., Pierre, T.S., Moroz, P., Jones, S., 2003. A magnetic resonance imaging based method for measurement of tissue iron concentration in liver arterially embolized with ferrimagnetic particles designed for magnetic hyperthermia treatment of tumors. *Magn. Reson. Imag.* 21, 483–488.
- Qin, L., Qiu, J., Liu, M., Ding, S., Shao, L., Lü, S., Zhang, G., Zhao, Y., Fu, X., 2011. Mechanical and thermal properties of poly (lactic acid) composites with rice straw fiber modified by poly (butyl acrylate). *Chem. Eng. J.* 166, 772–778.
- Rabinovich-Guilatt, L., Couvreur, P., Lambert, G., Goldstein, D., Benita, S., Dubernet, C., 2004. Extensive surface studies help to analyse zeta potential data: the case of cationic emulsions. *Chem. Phys. Lipids.* 131, 1–13.
- Raman, M., Doble, M., 2014. Physicochemical and structural characterisation of marine algae *Kappaphycus alvarezii* and the ability of its dietary fibres to bind mutagenic amines. *J. Appl. Phycol.* 26, 2183–2191.
- Sá, S., Gawande, M.B., Velhinho, A., Veiga, J.P., Bundaleski, N., Trigueiro, J., Tolstogousov, A., Teodoro, O.M., Zboril, R., Varma, R.S., 2014. Magnetically recyclable magnetite–palladium (Nanocat-Fe–Pd) nanocatalyst for the Buchwald-Hartwig reaction. *Green Chem.* 16, 3494–3500.
- Salazar-Alvarez, G., Muhammed, M., Zagorodni, A.A., 2006. Novel flow injection synthesis of iron oxide nanoparticles with narrow size distribution. *Chem. Eng. Sci.* 61, 4625–4633.
- Seigneuric, R., Markey, L., SA Nuyten, D., Dubernet, C., TA Evelo, C., Finot, E., Garrido, C., 2010. From nanotechnology to nanomedicine: applications to cancer research. *Curr. Mol. Med.* 10, 640–652.
- Şen, M., Erboz, E.N., 2010. Determination of critical gelation conditions of κ-carrageenan by viscosimetric and FT-IR analyses. *Food Res Int.* 43, 1361–1364.
- Shameli, K., 2013. Synthesis of talc/Fe₃O₄ magnetic nanocomposites using chemical co-precipitation method. *Int. J. Nanomed.* 8, 1817–1823.
- Shameli, K., Ahmad, M.B., Yunus, W., Ibrahim, N.A., Darroudi, M., 2010a. Synthesis and characterization of silver/talc nanocomposites using the wet chemical reduction method. *Int. J. Nanomed.* 5, 743–751.
- Shameli, K., Ahmad, M.B., Yunus, W.M.Z.W., Rustaiyan, A., Ibrahim, N.A., Zargar, M., Abdollahi, Y., 2010b. Green synthesis of silver/montmorillonite/chitosan bionanocomposites using the UV irradiation method and evaluation of antibacterial activity. *Int. J. Nanomed.* 5, 875–887.
- Shameli, K., Bin Ahmad, M., Jazayeri, S.D., Sedaghat, S., Shaban-zadeh, P., Jahangirian, H., Mahdavi, M., Abdollahi, Y., 2012. Synthesis and characterization of polyethylene glycol mediated silver nanoparticles by the green method. *Int. J. Mol. Sci.* 13, 6639–6650.
- Sisodiya, S., Wallenberg, L.R., Lewin, E., Wendt, O.F., 2015. Sonogashira coupling reaction over supported gold nanoparticles: Influence of support and catalyst synthesis route. *Appl. Catal. A-Gen.* 503, 69–76.
- Stampar, F., Solar, A., Hudina, M., Veberic, R., Colaric, M., 2006. Traditional walnut liqueur–cocktail of phenolics. *Food Chem.* 95, 627–631.
- Sun, X., Xu, F., Sun, R., Fowler, P., Baird, M., 2005. Characteristics of degraded cellulose obtained from steam-exploded wheat straw. *Carbohydr. Res.* 340, 97–106.
- Tan, W., Lu, J., Huang, M., Li, Y., Chen, M., Wu, G., Gong, J., Zhong, Z., Xu, Z., Dang, Y., 2011. Anti-cancer natural products isolated from Chinese medicinal herbs. *Chin. Med.* 6, 27.
- Tartaj, P., González-Carreño, T., Serna, C.J., 2004. From hollow to dense spheres: control of dipolar interactions by tailoring the architecture in colloidal aggregates of superparamagnetic iron oxide nanocrystals. *Adv. Mater.* 16, 529–533.
- Thakkar, K.N., Mhatre, S.S., Parikh, R.Y., 2010. Biological synthesis of metallic nanoparticles. *Nanomed. Nanotech. Biol. Med.* 6, 257–262.
- Venkateswarlu, S., Rao, Y.S., Balaji, T., Prathima, B., Jyothi, N., 2013. Biogenic synthesis of Fe₃O₄ magnetic nanoparticles using plantain peel extract. *Mater. Lett.* 100, 241–244.
- Vidal-Vidal, J., Rivas, J., López-Quintela, M., 2006. Synthesis of monodisperse maghemite nanoparticles by the microemulsion method. *Colloids Surf. A: Physicochem. Eng. Aspects* 288, 44–51.
- Vijayakumar, R., Koltypin, Y., Felner, I., Gedanken, A., 2000. Sonochemical synthesis and characterization of pure nanometer-sized Fe₃O₄ particles. *Mater. Sci. Eng., A.* 286, 101–105.
- Vincent, S., Kovendan, K., Chandramohan, B., Kamalakannan, S., Kumar, P.M., Vasugi, C., Praseeja, C., Subramaniam, J., Govindarajan, M., Murugan, K., 2017. Swift fabrication of silver nanoparticles using *Bougainvillea glabra*: potential against the Japanese encephalitis vector, *Culex tritaeniorhynchus* Giles (Diptera: Culicidae). *J. Cluster Sci.* 28, 37–58.
- Wu, W., He, Q., Jiang, C., 2008. Magnetic iron oxide nanoparticles: synthesis and surface functionalization strategies. *Nanoscale Res. Lett.* 3, 397.
- Yew, Y.P., Shameli, K., Miyake, M., Kuwano, N., Khairudin, N.B.B. A., Mohamad, S.E.B., Lee, K.X., 2016. Green synthesis of magnetite (Fe₃O₄) nanoparticles using seaweed (*Kappaphycus alvarezii*) extract. *Nanoscale Res. Lett.* 11, 1–7.
- Zhang, L., Yu, W., Han, C., Guo, J., Zhang, Q., Xie, H., Shao, Q., Sun, Z., Guo, Z., 2017. Large scaled synthesis of heterostructured electrospun TiO₂/SnO₂ nanofibers with an enhanced photocatalytic activity. *J. Electrochem. Soc.* 164, H651–H656.
- Zhao, D.-L., Teng, P., Xu, Y., Xia, Q.-S., Tang, J.-T., 2010. Magnetic and inductive heating properties of Fe₃O₄/polyethylene glycol composite nanoparticles with core–shell structure. *J. Alloy Compd.* 502, 392–395.